This is the Accepted Manuscript version of an article published in: International Journal of Energetic Materials and Chemical Propulsion, 15 (3): 249–274 (2016)
The Version of Record is available online at http://dx.doi.org/10.1615/IntJEnergeticMaterialsChemProp.2016013641

NUMERICAL MODELING OF COMBUSTION PROCESSES IN HYBRID ROCKET ENGINES

Alessandro Mazzetti[1] & Paolo Barbante[2,*]

[1]*Blue Think S.P.A., 20124 Milano, Italy*
[2]*Politecnico di Milano, Department of Mathematics, 20133 Milano, Italy*

[*]Address all correspondence to: Paolo Barbante, E-mail: paolo.barbante@polimi.it

Nowadays, numerical simulations of combustion processes in hybrid rockets are generally considered as a qualitative tool used mainly to describe the flow field inside the rocket engine. A research effort is of major importance in order to change this trend. It can be done by obtaining results that are quan-titatively accurate, to be used as a support for experimental research, reducing costs, and increasing efficiency in the development of better fuel formulations. The importance of such an effort relies on the fact that hybrid rockets are one of the most promising technologies in the aerospace propulsion field, with applications in hypersonic atmospheric flight, launch vehicles' upper stages, and space tourism, which is seen as a prelude for an economically feasible mass access to space. This is possible because of hybrid propulsion's low cost, intrinsic safety, and operational flexibility with potentially high per-formances. This research contribution aims to develop an accurate combustion model for traditional rubber-based hybrid rocket fuels (hydroxyl-terminated polybutadiene). Results of the simulations are presented as temperature distribution, axial velocity, and the products' mass fractions. A discussion about local and average fuel regression rates is presented, with particular attention to the effects on both the local and average regression rate, due to an increase in oxidizer mass flux and in pressure. Results of the present work suggest that an increase in oxidizer mass flux gives an increase in the average regression rate, while an increase in pressure gives a reduction in the average regression rate.

KEY WORDS: regression rate, hybrid rocket combustion, numerical modeling, turbulent combustion, partially stirred reactor (PaSR), GO2-HTPB system

1. INTRODUCTION

Hybrid rockets conjugate the best features of both liquid and solid rocket engines, e.g., ability to throttle and intrinsic safety with design simplicity and low cost. However, the low regression rate of traditional rocket fuels is still an important issue, because it leads to inadequate performance levels of the hybrid engine. Several techniques are able to face the challenge of obtaining a high regression rate, such as the use of high energetic materials (nanosized metals, metallic hydrides) or the use of nontraditional fuel for-mulations (liquefying paraffin-based fuels). The numerical modeling of the combustion process in hybrid rocket engines (HREs) is very challenging because of the complex physical mechanisms involved. The flowfield inside such an engine is turbulent, mul-

NOMENCLATURE

Acronyms

2D	two dimensional
3D	three dimensional
CFD	Computational fluid dynamics
COOLFluiD	Computational object oriented library for fluid dynamics
GMRES	Generalized minimum residual
HRE	Hybrid rocket engine
HTPB	Hydroxyl-terminated polybutadiene
MPI	Message passing interface
PaSR	Partially stirred reactor
PSR	Perfectly stirred reactor
PETSc	Portable, Extensible Toolkit for Scientific Computation

Roman Symbols

A	Arrhenius law pre-exponential constant [m^3/mol · s]
C	turbulence mixing time model constant
C_μ	turbulence model constant
c_p	specific heat at constant pressure [J/kg · K]
Ea	activation energy [cal/mol]
G_{Ox}	oxidizer mass flux [kg/m^2 · s]
h	enthalpy [J/kg]
J	laminar mass diffusion flux [kg/m^2 · s]
k	turbulence kinetic energy [m^2/s^2], Arrhenius constant
Le	Lewis number
M	molar mass [kg/mol]
Nr	number of chemical reactions
Ns	number of chemical species
Pr	Prandtl number
p	pressure [Pa]
R	universal gas constant [cal/mol · K]
r_b	regression rate [mm/s]
T	temperature [K]
t	time [s]
u	velocity component [m/s]
Y	chemical species mass fraction

Greek symbols

δ	Krönecker delta
Δh_0	formation enthalpy [J/kg]
Δh_{pf}	fuel pyrolisis enthalpy [J/kg]
κ	PaSR characteristic time ratio
λ	thermal conductivity [W/m · K]
μ	viscosity [Pa · s]
ν	stoichiometric coefficient
ρ	density [kg/m^3]
σ_k	turbulence kinetic energy model constant
σ_ω	turbulence frequency model constant
τ	laminar tress tensor [Pa]
τ_c	chemical reaction characteristic time [s]
τ_{mix}	turbulence mixing time [s]
τ^R	turbulent Reynolds stress tensor [Pa]
$\dot{\omega}$	chemical reaction mass source term
ω	turbulence frequency [s^{-1}]

tispecies, multiphase, reacting, with conductive, convective, and radiative heat transfer. Therefore the current research effort is mainly experimental. On the other hand, the development of a reliable and accurate numerical tool for the simulation of the behavior of hybrid rocket engines is of utmost importance. Two main achievements are possible by

numerical simulation of HREs. First, we can get an *a priori* estimation of hybrid rocket engine performance without the need of experimental testing, the latter being used as a comparison and validation technique. Second, the numerical modeling can enhance the development of innovative fuel formulations by reducing the number of experimental tests, therefore increasing the efficiency of research. Analytical investigations of hybrid rocket combustion have usually been based on the classical boundary-layer analysis of Marxman et al. (1963) to determine the heat flux to the fuel surface and consequently, the surface regression rate. Typically, the regression rate is given with simple correlations such as $r_b = aG_0^n$, where G_0 is the flow rate of the oxidizer and n is generally in the range 0.5–0.8. However, such simplified correlations cannot account for all the variations in operating conditions, chamber pressure, radiation, and finite-rate chemical kinetics. In particular, the model developed by Marxman et al. (1963) included the contribution of the radiation term to the hybrid rocket regression rate. The results were compared with Plexiglas combustion experiments: radiant heat transfer was quantified as 5–10% of total heat flux. Chiaverini et al. (2000) proposed a model with a modified radiation term in order to better fit experimental results. Nevertheless, such simplified models are limited to providing qualitative trends and are not adequate for giving quantitative data. Venkateswaran and Merkle (1996) developed a computational model for hybrid rocket flow-field simulation. The focus of this model is on the characterization of the fuel regression rate by comparing and calibrating the numerical data using the experimental results by Chiaverini and co-workers (Chiaverini et al., 2000; 2007). All the computational results shown in Venkateswaran and Merkle (1996) are two dimensional and obtained using a quasi-steady assumption, e.g., the fuel port dimensions were held fixed at values corresponding to different burning stages. Steady-state solutions were used to provide the instantaneous burning rates at the operating conditions. The quasi steady assumption is adequate because the fuel surface regression rate is typically much smaller than the axial velocity in the port. A recent study by Coronetti and Sirignano (2013) predicts the regression rate of the hydroxyl-terminated polybutadiene (HTPB)/gaseous oxygen formulation and its sensitivities to some operating parameters, such as combustion chamber pressure, oxygen inlet temperature, and mass flow rate. Hu et al. (2013) develop a numerical model to predict the regression rate for the solid fuel surface of the hybrid rocket motor under different operation conditions. The multidimensional Favre-averaged compressible turbulent Navier-Stokes equations are used as the governing equations of the reacting flow, the two-equation turbulence model is used to simulate the turbulent flow, and the eddy breakup model is used to simulate the gas combustion. The results presented are for hydroxyl-terminated polybutadiene fuel and gaseous oxygen. The model predictions indicate that fuel surface regression rates are considerably impacted by both the size and geometry of the configuration. Other recent works focus on specific aspects of HRE modeling. For example, Li et al. (2013) focus on three-dimensional numerical simulations of HRE with hydrogen peroxide (HP) and hydroxyl-terminated polybutadiene propellant combination and

investigates the fuel regression rate distribution characteristics of different fuel types. Simulation results, including the temperature contours and fuel regression rate distributions, are presented for different grain geometries. Chen et al. (2011) present a numerical model with real-fluid properties and finite-rate chemistry to predict the combustion flow field inside a N_2O-HTPB hybrid rocket system. A very recent contribution by Sun et al. (2012) attempts to research and predict the effect of the aluminum particle additives on the performance of the HTPB/98HP hybrid rocket motor with a numerical approach. Despite the large amount of research (mostly qualitative) ongoing in the field, the computational fluid dynamics (CFD) models of hybrid rocket engines need to be improved (Kuo and Houim, 2011). In particular, further investigation is needed in order to model multiphase flows, turbulence, and solid-gas-phase interface combustion and radiation.

2. PHYSICAL MODEL

The flow field inside a hybrid rocket is turbulent, multispecies, multiphase, and chemically reacting. Direct numerical simulation is computationally unfeasible and also, large eddy simulation is too demanding for full-scale simulations. For this reason, Reynolds-averaged equations have been chosen as an acceptable compromise between model accuracy and computational efforts. The Favre average is applied in order to avoid the modeling of density fluctuation correlations (Gatski and Bonnet, 2009), which is present when applying the usual Reynolds average. The Favre average is denoted by the tilde symbol, whereas an overbar denotes the usual Reynolds average. The Favre-averaged, unsteady, viscous, compressible Navier-Stokes governing equations used are detailed in the present section. Species continuity equations are added in order to account for multispecies, turbulent combustion conditions. In this paper the Einstein convention on repeated indexes is used.

Continuity equation:

$$\frac{\partial \overline{\rho}}{\partial t} + \frac{\partial}{\partial x_j}\left(\overline{\rho}\tilde{u}_j\right) = 0 \tag{1}$$

Species continuity equations ($k = 1 \ldots Ns$):

$$\frac{\partial}{\partial t}\left(\overline{\rho}\tilde{Y}_k\right) + \frac{\partial}{\partial x_j}\left(\overline{\rho}\tilde{u}_j\tilde{Y}_k\right) = -\frac{\partial}{\partial x_j}\left(\overline{\rho}\widetilde{u_j''Y_k''}\right) - \frac{\partial \overline{J}_j^k}{\partial x_j} + \overline{\dot{\omega}}_k \tag{2}$$

Momentum equation:

$$\frac{\partial}{\partial t}\left(\overline{\rho}\tilde{u}_i\right) + \frac{\partial}{\partial x_j}\left(\overline{\rho}\tilde{u}_j\tilde{u}_i\right) = -\frac{\partial}{\partial x_j}\left(\overline{\rho}\widetilde{u_i''u_j''}\right) - \frac{\partial \overline{p}}{\partial x_i} + \frac{\partial \overline{\tau}_{ji}}{\partial x_j} \tag{3}$$

Total energy equation:

$$\frac{\partial}{\partial t}\left(\overline{\rho}\tilde{e}_t\right)+\frac{\partial}{\partial x_j}\left(\overline{\rho}\tilde{u}_j\tilde{h}_t\right)+\frac{\partial \overline{q}_j}{\partial x_j}=-\frac{\partial}{\partial x_j}\left(\overline{\rho}\widetilde{u_j''h_t''}\right)+\frac{\partial}{\partial x_j}\left(\tilde{u}_i\overline{\tau}_{ji}\right)+\frac{\partial}{\partial x_j}\left(\overline{u_i''\tau_{ji}}\right) \quad (4)$$

Favre-averaged total energy includes the turbulence kinetic energy k and is defined as $\tilde{e}_t=\tilde{e}+\frac{1}{2}\tilde{u}_i\tilde{u}_i+k$; Favre-averaged total enthalpy $\tilde{h}_t$ is equal to $\tilde{e}_t+\overline{p}$.

Turbulence closure is modeled with the Wilcox $k-\omega$ model (Wilcox, 2006). Turbulence kinetic energy equation:

$$\frac{\partial}{\partial t}\left(\overline{\rho}k\right)+\frac{\partial}{\partial x_j}\left(\overline{\rho}\tilde{u}_j k\right)=P-\beta^*\overline{\rho}\omega k+\frac{\partial}{\partial x_j}\left[\left(\mu+\sigma^*\frac{\overline{\rho}k}{\omega}\right)\frac{\partial k}{\partial x_j}\right] \quad (5)$$

Specific dissipation rate equation:

$$\frac{\partial}{\partial t}\left(\overline{\rho}\omega\right)+\frac{\partial}{\partial x_j}\left(\overline{\rho}\tilde{u}_j\omega\right)=\alpha\frac{\omega}{k}P-\beta\overline{\rho}\omega^2+\frac{\partial}{\partial x_j}\left[\left(\mu+\sigma\frac{\overline{\rho}k}{\omega}\right)\frac{\partial \omega}{\partial x_j}\right] \quad (6)$$

where P is defined as

$$P=\tau_{ij}^R\frac{\partial \tilde{u}_i}{\partial x_j} \quad (7)$$

and $\tau_{ij}^R=-\overline{\rho}\widetilde{u_i''u_j''}$ is the turbulent Reynolds stress tensor. The specific values of the closure coefficients β^*, σ^*, α, β, and σ that appear in Eqs. (5) and (6) can be found in Wilcox (2006).

3. PHYSICAL MODEL CLOSURE

Laminar diffusion fluxes can be rigorously computed by solving the Stefan-Maxwell equations' linear system (Ferziger and Kaper, 1972) of dimension Ns by Ns. A computationally cheaper approach that still ensures the conservation of mass is the modified Fick's law of Ramshaw (1990). An ever simpler approach that satisfies mass conservation is Fick's law with a constant Lewis number (Le). All the chemical species have the same diffusion coefficient which is equal to $D=\lambda/(\rho c_p \mathrm{Le})$. In this paper we have selected the third approach for the computation of laminar diffusion fluxes with $\mathrm{Le}=1.4$. The averaged laminar diffusion flux reads

$$\overline{J}_j^k=-\overline{\rho D\frac{\partial Y_k}{\partial x_j}}=-\overline{\rho}\tilde{D}\frac{\partial \tilde{Y}_k}{\partial x_j} \quad (8)$$

where the term $\widetilde{D''\partial Y_k''}/\partial x_j$ has been neglected (Gatski and Bonnet, 2009). The averaged laminar viscous stress tensor reads

$$\overline{\tau}_{ij} = \tilde{\mu}\left(\frac{\partial \tilde{u}_i}{\partial x_j} + \frac{\partial \tilde{u}_j}{\partial x_i} - \frac{2}{3}\frac{\partial \tilde{u}_k}{\partial x_k}\delta_{ij}\right) \tag{9}$$

where again we have neglected products of fluctuations of viscosity and of velocity (Gatski and Bonnet, 2009). Finally the averaged laminar heat flux, still neglecting products of fluctuations (Gatski and Bonnet, 2009), reads

$$\overline{q}_j = -\tilde{\lambda}\frac{\partial \tilde{T}}{\partial x_j} + \sum_{k=1}^{Ns} \overline{J}_j^k \tilde{h}_k \tag{10}$$

$\tilde{h}_k$ being the averaged enthalpy of species k.

The turbulent transport of mass term, $\overline{\rho}\widetilde{u_j'' Y_k''}$, is closed with a gradient hypothesis, defining turbulent Prandtl and Lewis numbers ($\mathrm{Pr}_T \approx 0.7 - 0.9$, $\mathrm{Le}_T \approx 1.0 - 1.4$), as shown in Eq. (11):

$$\overline{\rho}\widetilde{u_j'' Y_k''} = -\frac{\mu_T}{\mathrm{Pr}_T \mathrm{Le}_T}\frac{\partial \tilde{Y}_k}{\partial x_j} \tag{11}$$

$\mathrm{Pr}_T = 0.9$ and $\mathrm{Le}_T = 1.0$ were chosen for the computations shown in this paper.
The Reynolds stress tensor, $-\overline{\rho}\widetilde{u_i'' u_j''}$, is computed with the eddy viscosity hypothesis (Wilcox, 2006):

$$\tau_{ij}^R = -\overline{\rho}\widetilde{u_i'' u_j''} = \mu_T\left(\frac{\partial \tilde{u}_i}{\partial x_j} + \frac{\partial \tilde{u}_j}{\partial x_i} - \frac{2}{3}\frac{\partial \tilde{u}_k}{\partial x_k}\delta_{ij}\right) - \frac{2}{3}\overline{\rho}k\delta_{ij} \tag{12}$$

In literature, Veynante and Vervisch (2002), as well as Veynante and Poinsot (2011), proposed a simple closure for the turbulent transport of total enthalpy term, $\overline{\rho}\widetilde{u_i'' h_t''}$, as $c_p \nabla T$. However, in this work a more accurate, new approach is introduced. In fact, the exact expression for turbulent transport of total enthalpy, from the mass-averaged energy balance equation (4), is

$$\begin{aligned}\overline{\rho}\widetilde{u_j'' h_t''} = &\underbrace{\sum_{k=1}^{Ns}\left[\overline{\rho}\widetilde{u_j'' Y_k''}\left(\tilde{h}_s^k + \Delta h_0^k\right)\right]}_{1} + \underbrace{\sum_{k=1}^{Ns}\overline{\rho}\widetilde{u_j'' Y_k h_s^k}''}_{2} - \underbrace{\tilde{u}_i \tau_{ji}^R}_{3} \\ &+ \underbrace{\overline{\rho}\widetilde{u_j''\frac{1}{2}u_i'' u_i''}}_{4}\end{aligned} \tag{13}$$

where h_s^k is the thermodynamic sensible enthalpy of species k and Δh_0^k is its formation enthalpy. The terms appearing in Eq. (13) are stated respectively. Term 1 represents the transport of averaged thermodynamic enthalpy (sum of sensible enthalpy and formation enthalpy) by means of the turbulent transport of mass term, $\overline{\rho}\widetilde{u_j'' Y_k''}$, that appears

in Eq. (2). Term 2 represents the turbulent flux of mixture sensible enthalpy. Term 3 represents the work performed by the Reynolds stress tensor. Term 4 is related to the transport of turbulence kinetic energy by velocity fluctuations. Model self-consistency requires to close term 1 by means of Eq. (11) and not with a gradient-type hypothesis. Term 2 instead can be closed with a gradient hypothesis, term 3 is computed exactly by means of Eq. (12), term 4 is summed with $\overline{u_i''\tau_{ji}}$, and the two are closed with a gradient hypothesis (Wilcox, 2006). Equation (13) now reads

$$\widetilde{\overline{\rho}u_j''h_t''} + \overline{u_i''\tau_{ji}} = \underbrace{-\sum_{k=1}^{Ns}\frac{\mu_T}{\mathrm{Pr}_T\mathrm{Le}_T}\frac{\partial\tilde{Y}_k}{\partial x_j}\left(\tilde{h}_s^k + \Delta h_0^k\right)}_{1} \underbrace{-\frac{\mu_T}{\mathrm{Pr}_T}\frac{\partial\tilde{h}_s}{\partial x_j}}_{2} + \underbrace{\tilde{u}_i\tau_{ji}^R}_{3} + \underbrace{\left(\mu + \frac{\mu_T}{\sigma^*}\right)\frac{\partial k}{\partial x_j}}_{4} \tag{14}$$

where $\tilde{h}_s$ is the averaged sensible enthalpy of the mixture.

3.1 Chemistry Closure

This work uses two different closure models for the source term of chemical reactions. The first one, as in Venkateswaran and Merkle (1996), considers chemical reactions in a pseudo-laminar condition, the perfectly stirred reactor (PSR) hypothesis. The second one, as in Golovitchev (2001), corrects the pseudolaminar model by chemistry and turbulence characteristic times in order to obtain a fully turbulent representation of the chemistry source term. This is the partially stirred reactor (PaSR) approach. The schemes will be discussed in the next two sections.

3.1.1 Perfectly Stirred Reactor

In the PSR model, the effect of fluctuations of species mass fractions and temperature is neglected and the chemical source term for the kth species reads

$$\overline{\dot{\omega}}_k = M_k\sum_{r=1}^{Nr}\left(\nu_{k,r}'' - \nu_{k,r}'\right)\overline{\dot{\omega}}_r = M_k\sum_{r=1}^{Nr}\left(\nu_{k,r}'' - \nu_{k,r}'\right) \times \left\{k_{f,r}\prod_{i=1}^{Ns}\left[\frac{\overline{\rho}\tilde{Y}_i}{M_i}\right]^{\nu_i'} - k_{b,r}\prod_{i=1}^{Ns}\left[\frac{\overline{\rho}\tilde{Y}_i}{M_i}\right]^{\nu_i''}\right\} \tag{15}$$

This model is valid only when the characteristic time of turbulent mixing is much shorter than the characteristic time of chemistry and the chemical composition is practically homogeneous in every computational cell.

3.1.2 Partially Stirred Reactor (PaSR)

In order to obtain more accurate results for turbulence-chemistry interaction, a partially stirred reactor approach is also implemented. Initially proposed by Golovitchev (2001), the PaSR model overcomes the simplified approach given by a pseudo-laminar chemistry by considering that only a fraction of the volume of each computational cell is affected by the presence of a chemically reacting zone. The reacting volume fraction of each computational cell is proportional to the ratio κ of chemical reaction time τ_c and total time $\tau_c + \tau_{\mathrm{mix}}$, as shown in Golovitchev and Chomiak (2001) (τ_{mix} is the turbulent mixing time). The chemistry source term is modified using the aforementioned time ratio κ, as

$$\overline{\dot{\omega}}_{k,T} = \kappa \overline{\dot{\omega}}_k = \frac{\tau_c}{\tau_c + \tau_{\mathrm{mix}}} \overline{\dot{\omega}}_k \tag{16}$$

It can be noticed that when $\tau_{\mathrm{mix}} \ll \tau_c$ the PSR model is recovered. Several definitions for these characteristic times are possible, as proposed by Golovitchev (2001), Golovitchev and Chomiak (2001), Nordin (2001), or Sabelnikov and Fureby (2013). The cited references all propose the choice of a single chemistry characteristic time τ_c. However, choosing a common time for several chemical reactions, which might have different characteristic times, can be difficult, and a poor choice of the common time could degrade the model accuracy. In this work we have tried to overcome this problem with a multitime PaSR model. For each chemical reaction a characteristic time is chosen from the chemical system Jacobian matrix, therefore representing the sensitivity of a chemical reaction to variations in concentration of a given species. For the rth reaction the characteristic time $\tau^r_{c,k}$ associated with the variation of kth chemical species partial density (or concentration, being these two quantities strictly linked) is

$$\frac{1}{\tau^r_{c,k}} = \frac{\partial \overline{\dot{\omega}}_r \left(\rho_1 \cdots \rho_{Ns}, T\right)}{\partial \rho_k} \tag{17}$$

where $\overline{\dot{\omega}}_r$ is defined in Eq. (15). Among all the characteristic times $\tau^r_{c,k}$, the minimum one is chosen as a characteristic time of the rth reaction. This specific choice is made by considering that in the PaSR model the influence of turbulence is greater for small chemical times. On the other hand, if the chemistry time is large enough, the volume fraction κ is not influenced by turbulence because τ_{mix} becomes negligible with respect to τ_c and κ is close to unity. Therefore, within the PaSR framework, the fastest chemical reactions (small chemical time) are more influenced by turbulence, while the slowest chemical reactions (large chemical time) are less affected by turbulence. The use of a too large τ_c for a given reaction scheme might unphysically make the turbulent mixing time negligible; this results in a PaSR approach that actually falls back into PSR. For the considered reaction scheme (see Section 3.1.3), the multitime PaSR model results in a characteristic chemical time for each one of the six reactions involved.

The turbulent mixing time is chosen according to Nordin (2001); therefore

$$\tau_{\mathrm{mix}} = C\frac{k}{\epsilon} = \frac{C}{C_{\mu}\omega} \tag{18}$$

C being a model constant, with values ranging from 0.001 to 0.03. The value chosen for this work is 0.005 (Nordin, 2001; Amini and Khalegi, 2011). C_{μ} is the turbulence model constant 0.09 (Wilcox, 2006).

3.1.3 Reaction Scheme

The six reaction, nine species global reaction mechanism from Jones (1983) is chosen as a compromise between the number of chemical species involved and the computational cost. This model considers gaseous butadiene as the only pyrolisis product of solid HTPB, which is in agreement with the work of Risha et al. (1998). Arrhenius-type reaction rate coefficients are used and are expressed as

$$k = AT^{n}\exp\left(-\frac{Ea}{RT}\right) \tag{19}$$

The chemical kinetics model is reported in Table 1.

4. GAS-SOLID FUEL INTERFACE BOUNDARY CONDITION

In order to estimate fuel regression rate of pyrolizing HTPB, it is necessary to implement an adequate boundary condition at the interface between the gas fluid domain and the solid fuel grain. In order to achieve a physically consistent and accurate formulation, the boundary condition is analytically derived using a two-phase approach according to Kataoka (1986). Three main assumptions were made: first, no diffusion is present inside the solid fuel; second, the bulk of the solid fuel is not moving, and finally, no surface chemical reactions are present at the gas-solid fuel interface, like, for example, reactions promoted by heterogeneous catalysis. Several contributions are neglected in the

TABLE 1: Chemical reaction scheme

Reaction	A	Ea [cal/mol]	n	Reaction Rate	a	b
(1) C_4H_6+2O_2 $\longleftrightarrow$ 4CO+3H_2	3.08×10^{08}	–30000	0	$k_1[C_4H_6]^a[O_2]^b$	0.5	1.25
(2) C_4H_6+H_2O $\longleftrightarrow$ 4CO+7H_2	3.79×10^{11}	–30000	0	k_2 $[C_4H_6]^a[H_2O]^b$	1.00	1.00
(3) CO+H_2O $\longleftrightarrow$ CO_2+H_2	2.75×10^{09}	–20000	0	$k_3[CO]^a[H_2O]^b$	1.00	1.00
(4) H_2+0.5O_2 $\longleftrightarrow$ H_2O	7.50×10^{15}	–40000	–1	$k_4[H_2]^a[O_2]^b$	0.25	1.50
(5) O_2+M $\longleftrightarrow$ O+O+M	1.50×10^{09}	–113000	0	$k_5[O_2]^a$	1.00	—
(6) H_2O+M $\longleftrightarrow$ OH+H+M	2.30×10^{22}	–120000	–3	$k_6[H_2O]^a$	1.00	—

energy boundary condition at the gas-solid fuel interface: the work of viscous stresses, kinetic energy flux, and radiation. The work of viscous stresses and the kinetic energy flux are negligible for combustion flow conditions because their contribution is much smaller than fuel pyrolisis enthalpy. The introduction of a model for radiation that can contribute up to 5–10% of the total heat flux (Marxman et al., 1963), is considered as a next step for future development of the current model. The contribution of radiation is mandatory when solid fuel formulations include particulate (either metals or soot) or are additivated with carbon black (in order to increase radiation heat flux back to the fuel grain). However, in our case the fuel is pure HTPB and the radiation contribution can be neglected. In this section, bold symbols denote vectorial quantities.

Mass balance for the full mixture at the gas-solid fuel interface reads:

$$\mathbf{v}_g \cdot \mathbf{n} = -\frac{\rho_f - \rho_g}{\rho_g}\mathbf{v}_I \cdot \mathbf{n} = \frac{\rho_f - \rho_g}{\rho_g} r_b \tag{20}$$

where subscript g stands for gas phase and subscript f for solid fuel; $\mathbf{n}$ is the normal to the gas-solid fuel interface, $\mathbf{v}_g$ is the gas phase velocity vector, $\mathbf{v}_I$ is the gas-solid fuel interface velocity. We notice that the bulk of the solid fuel is fixed, but the interface is moving. $\mathbf{v}_I$ is determined by the fuel regression rate: $\mathbf{v}_I \cdot \mathbf{n} = -r_b$.

Energy balance at the gas-solid fuel interface gives

$$\rho_f h_g r_b - \lambda_g \nabla T_g \cdot \mathbf{n} + \left(\sum_{i=1}^{Ns} \mathbf{J}_{g,i} h_{g,i} \right) \cdot \mathbf{n} = \rho_f r_b (h_{gf} - \Delta h_{pf}) - \lambda_f \nabla T_f \cdot \mathbf{n} \tag{21}$$

where h_{gf} is the fuel enthalpy in its gaseous state and Δh_{pf} the fuel pyrolisis enthalpy.

Taking into account that there are no surface chemical reactions at the interface and that the fuel is made of pure HTPB, the mass fraction boundary condition is written

$$\mathbf{J}_{g,i} \cdot \mathbf{n} = \begin{cases} (Y_{f,i} - Y_{g,i})\rho_f r_b & \text{if i = fuel} \\ -Y_{g,i}\rho_f r_b & \text{else} \end{cases} \tag{22}$$

Equations (20), (21), and (22) constitute a nonlinear system with respect to mass fractions, temperature, and velocity components $\mathbf{v}_g \cdot \mathbf{n}$, where the unknowns are all located at the gas-solid fuel interface. Therefore, an iterative solution procedure for solving this system has to be applied. The closure of this nonlinear problem requires also a model for the fuel pyrolisis law. This is obtained by applying an Arrhenius-type law from Chiaverini et al. (1999):

$$r_b = A \exp\left(-\frac{E_a}{RT_f}\right) \begin{cases} A = 11.04 \text{ mm/s}, & E_a = 4.91 \text{ kcal/mol} \quad \text{if } T \geq 722\text{K} \\ A = 3965 \text{ mm/s}, & E_a = 13.35 \text{ kcal/mol} \quad \text{if } T < 722\,\text{K} \end{cases} \tag{23}$$

The previous law is based on 1 bar operative conditions; however, it is reasonable to assume (Evans et al., 2009) that, at least for $T >$ 850-900 K, there is no significant effect of pressure. Solid fuel data such as density and pyrolisis enthalpy are also needed to fully close the boundary problem. These are shown in Table 2 and are collected from SPLab work (Merotto et al., 2011), where a study of traditional butadiene-based and innovative paraffin-based fuels is described. In addition, in order to obtain the gradient of solid fuel temperature at the interface, the one-dimensional heat conduction problem is analytically solved inside the solid fuel (Cai et al., 2013) (y being the coordinate locally perpendicular to the gas-solid fuel interface).

$$T(y) = T_0 + (T_f - T_0) \exp\left(-\frac{\rho_f c_f r_b y}{\lambda_f}\right) \tag{24}$$

T_0 is the temperature of the fuel grain that is far from the gas-solid interface; in the computations it has been assumed $T_0 = 300$ K. At the interface, where $y = 0$, the temperature gradient is

$$-\lambda_f \nabla T_f \cdot \mathbf{n} = \rho_f c_f r_b (T_f - T_0) \tag{25}$$

5. COOLFLUID COMBUSTION CODE

The system of equations previously introduced is implemented in the COOLFluiD object-oriented scientific computing environment, developed at von Karman Institute for Fluid Dynamics [see Lani (2008); Quintino (2008); and Wuilbaund (2008)]. This is an MPI parallel code, constituted by a kernel with a dynamic plugins structure which solves multiple physical models (on 2D and 3D meshes) and offers multiple discretization techniques (finite differences, finite elements, and finite volumes). In order to solve the multispecies, turbulent reacting flow for the modeling of HRE, a specific mix of existing or realized ad-hoc plugins was chosen. The Navier-Stokes system of equations is discretized with a second-order accurate cell-centered finite volume method. The convective terms are discretized with the Liou (2006) AUSM+-Up flux-splitting scheme. Diffusive fluxes, which are also dependent on variable gradients, are calculated by nodal extrapolation on a diamond-shaped volume, as described in Lani (2008). Source terms

TABLE 2: Solid fuel data used in this work

Solid fuel data		
Property	**Symbol**	**Value**
Fuel density	ρ_f	960 kg/m^3
Specific heat	c_f	2860 J/kg K
Pyrolisis enthalpy	Δh_{pf}	1100000 J/kg
Thermal conductivity	λ_f	0.217 W/m K
Fuel temperature, far from interface	T_0	300 K

are discretized in the same fashion as diffusive fluxes but using cell center values and cell volume (instead of diamond-shaped volumes). An implicit Euler discretization scheme is used for time advancement until steady state is reached. The resulting linear system is solved using PETSc (Balay et al., 1997) libraries with the generalized minimum residual (GMRES) technique.

6. RESULTS AND DISCUSSION

The computations were performed on a two-dimensional domain whose geometry reproduces the inner combustion liner from SPLab facilities at Politecnico of Milano (Mazzetti, 2010). The computational domain represents the combustion chamber of a hybrid rocket, in particular, considering ideally the central section of the combustor. A sketch of the combustion chamber is shown in Fig. 1; the y direction is stretched for sake of clarity. The chamber is rectangular: 6 mm high (transverse direction) and 125 mm long (axial direction). In the head-end section, injector/swirlers and pre-burners are not included in the computational domain. Thus the domain starts just after the oxidizer flux is assumed to be made fully turbulent by the injection system. A transverse inlet for fuel is present in the lower wall of the combustion chamber. The fuel inlet starts at a distance of 25 mm from the oxidizer inlet and is 50 mm long. The computational domain extends up to 50 mm after the fuel inlet end, with an outlet boundary at fixed pressure. Thus the domain ends after the combustor section and does not include a nozzle. A good compromise between accuracy, boundary layer resolution, and computational time is

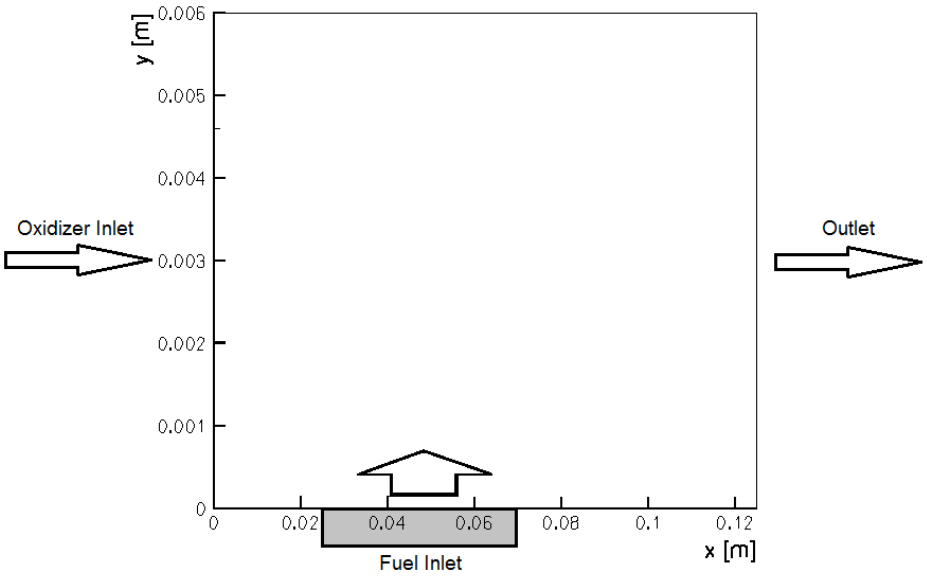

FIG. 1: Sketch of the combustion chamber.

granted by an 8000 cell mesh, with 80 cells in height and 100 cells in width. Boundary conditions are summarized in Table 3, with turbulence considered to be fully developed at oxidizer and fuel inlets. Physical walls, outside of the fuel inlet region, are reproduced by isothermal no-slip walls.

6.1 Temperature, Speed, and Product Mass Fractions

Computations are performed for different pressure and oxidizer mass flux conditions in order to assess their effect on the flame and combustion parameters. In particular, pressures of 1, 2.5, 5, and 10 bar are investigated. Each pressure case is investigated for increasing oxidizer mass flux: 1 bar case is investigated for 8, 13, 19, 26, 33, 39, 46, and 52 kg/m^{2}s oxidizer inlet mass flux; 2.5 bar case is investigated for 19, 39, 52, and 65 kg/m^{2}s oxidizer inlet mass flux; 5 bar case is investigated for 19, 39, 65, and 98 kg/m^{2}s oxidizer inlet mass flux; 10 bar case is investigate for 39, 78, 130, and 195 kg/m^{2}s oxidizer mass flux.

Results are presented in Figs. 2–6, where profiles of temperature, axial velocity, and chemical compositions are shown at several transverse sections inside the combustion chamber. This set refers to fully turbulent boundary conditions with 10 bar pressure and 39 kg/m^{2}s oxidizer mass flux. The results for the other pressure and oxidizer mass flux conditions are qualitatively similar to the ones shown in Figs. 2–6. Figure 2 shows the temperature profiles at different sections along the modeled combustion chamber; the maximum temperature is located above the fuel inlet. The temperature peak, near 3250 K, and the flame geometry are coherent with the nature of the turbulent combustion problem. The shape of the peak temperature region corresponds effectively to a turbulent flame, whereas laminar flames are characterized by a narrower profile, as in Venkateswaran and Merke (1996) and in Law (2006). In fact, with the PaSR approach, only a fraction of each computational cell takes part in the combustion process.

TABLE 3: Boundary conditions[a]

Boundary	u **[m/s]**	v **[m/s]**	T **[K]**	k $[\mathbf{m^2/s^2}]$	$\boldsymbol{\omega}[\mathbf{s^{-1}}]$	p **[Pa]**
Oxidizer inlet	case dependent	0	300	1×10^{-4}	1.11×10^{8}	—
Fuel inlet	0	rb dependent	Energy balance	1×10^{-4}	1.11×10^{8}	—
Upper wall	0	0	300	0	wall law[a]	—
Lower wall – pre-inlet	0	0	300	0	wall law[a]	—
Lower wall – post-inlet	0	0	600	0	wall law[a]	—
Outlet	—	—	—	—	—	101325

[a]Wall law from Menter's $k - \omega$ model (Menter, 1994).

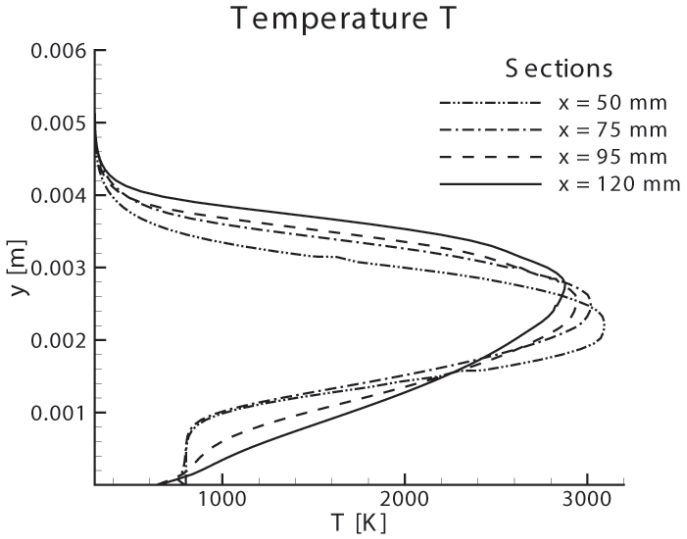

FIG. 2: Temperature section profiles: p = 10 bar, GOx = 39 kg/m^{2}s.

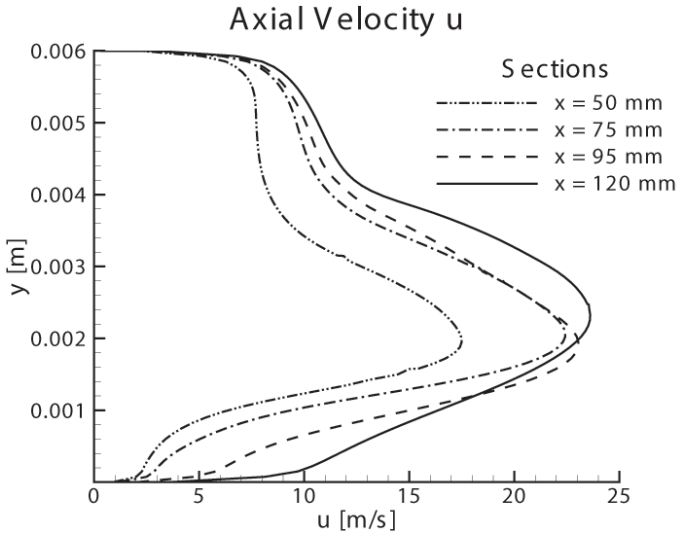

FIG. 3: Axial velocity section profiles: p = 10 bar, GOx = 39 kg/m^{2}s.

Therefore, oxidizer and fuel species do not fully react inside each cell as with the PSR approach, but a part of them is transported further by molecular diffusion and by turbulence. This process creates a wider zone where the oxidizer-fuel ratio is still adequate for sustaining the combustion process. Figure 3 shows the axial velocity profiles at several locations along the combustor. As expected, an axial acceleration of the fluid

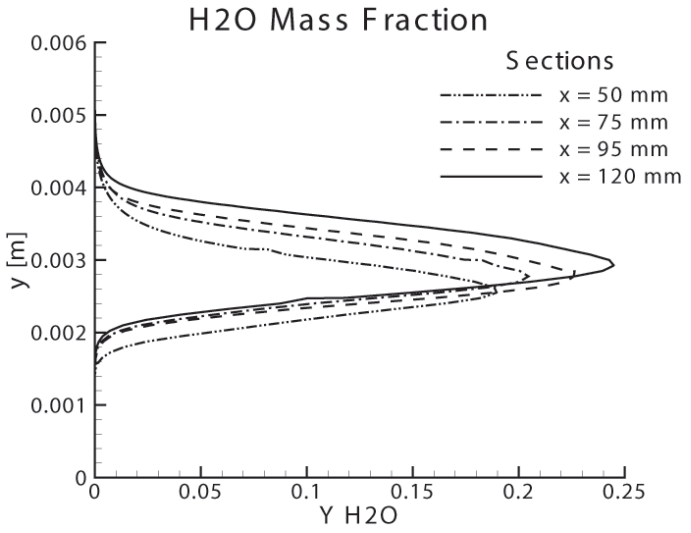

FIG. 4: H_2O Mass fraction section profiles: p = 10 bar, GOx = 39 kg/m^{2}s.

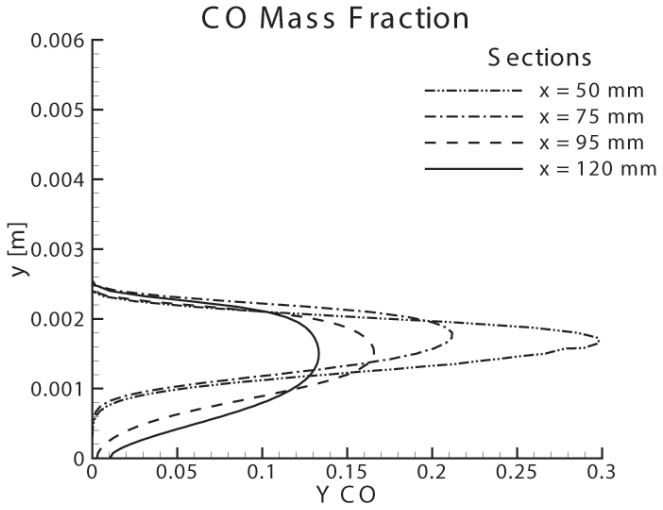

FIG. 5: CO Mass fraction section profiles: p = 10 bar, GOx = 39 kg/m^{2}s.

is observed, with a peak near 24 m/s (oxidizer inlet velocity is 3 m/s for this case). Figures 4–6 show the section profiles for the main combustion products: H_2O, CO, and CO_2. It is noticeable how the peak of combustion products follows the temperature peak, as expected from the chemical reaction scheme. CO_2, which appears in the chemical model only as a reaction product, is generated homogeneously along the flame. It is also possi-

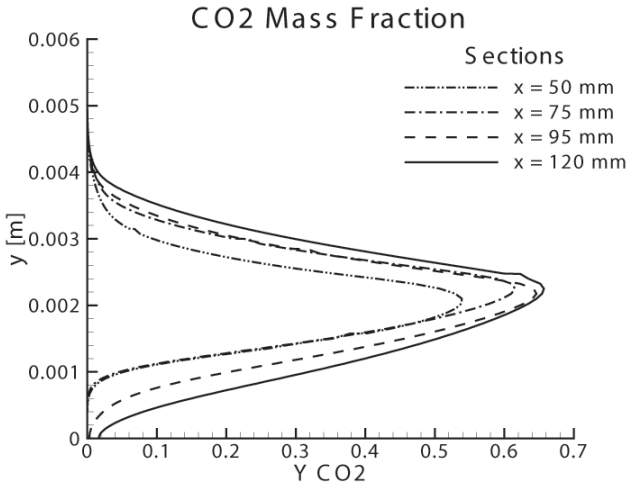

FIG. 6: CO_2 Mass fraction section profiles: p = 10 bar, G_{Ox} = 39 kg/m^{2}s.

ble to notice a separation between the regions where H_2O and CO_2 are present, because H_2O is a reactant in the production of CO_2 (see the third reaction in Table 1).

6.2 Regression Rate Evaluation

The fuel regression rate is the main parameter used to assess hybrid rocket performances and to comparatively evaluate different fuel formulations. The previously described boundary condition is used within the simulation code to estimate fuel regression rate for the pressure and oxidizer mass flux conditions detailed in Section 6.1. It is important to point out that determining an overall behavior of combustion in hybrid rockets under the effects of different pressure conditions is still an open question in the research community. The regression rate trend at different pressure conditions is particularly important. In general, for standard operating conditions of hybrid rockets, the regression rate is considered to be slightly or not affected by pressure, as stated by Evans et al. (2009) and Lewin et al. (1992). On the other hand, previous work from Price and Smoot (1965) describes the complex behavior of regression rate based on three different oxidizer mass flux conditions (low, intermediate, and high) and three pressure regimes (low, medium, and high). The work from Price and Smoot (1965), with 10–120 kg/m^{2}s oxidizer mass flux range and 1.4–11 bar pressure, shows that the pressure effect on regression rate is negligible at low oxidizer mass flux and it is increasingly stronger with increasing oxidizer mass flux; for high mass fluxes the regression rate should increase with pressure. More recent work from Yash et al. (2011) also shows an increase in regression rate with pressure. On the other hand, the work of Risha et al. (1998) shows a decrease in regression rate with increasing operating pressure. This work is based on ex-

perimental pyrolisis tests inside a windowed combustor and cannot be truly considered as a regression rate evaluation test for a real hybrid rocket engine. Pressure conditions were ranging from 7.9 to 35.5 bar, while the total oxidizer mass flow rate is between 0.001 and 0.002 kg/s. In the present work, a similar behavior is identified in all pressure conditions at varying oxidizer mass flux.

Some general considerations can be drawn from the case p = 1 bar shown in Figs. 7 and 8. We show the temperature (Fig. 7) and the fuel regression rate (Fig. 8) for the following values of the oxidizer mass flow rate G_{Ox}: 8, 13, 26, 52 kg/m^{2}s. They correspond to an inlet velocity U_{Ox} of 6, 12, 20, 40 m/s, respectively. Noticeably, the regression rate is not constant along the fuel grain but has a peak in the fuel grain head-end. This corresponds to the peak in fuel surface temperature and it is coherent with the presence of the hotter flame zone very close to the fuel in the head-end region (see Fig. 2). It is also in agreement with experimental results, as shown in De Luca et al. (2011). Moreover, an increase of oxidizer inlet velocity corresponds to an increase of fuel temperature and therefore regression rate at the fuel grain head-end. Overall the results are consistent with the modeling assumptions introduced. However a large-eddy simulation (LES) model would be more accurate than our RANS approach for the modeling of the typical recirculation region at the fuel inlet that our boundary condition does not take into account. In addition, the extrapolation of the pyrolisis law of Eq. (23) from 1 bar to the whole pressure range might reduce the accuracy of the present model for the section of the fuel slab with a surface temperature below 850 K. Moreover, the fuel layer where pyrolisis takes place is assumed to be vanishingly thin and located at the gas-solid fuel interface. Subsurface pyrolisis is neglected, and this could be important for low oxidizer mass flow rate conditions, because it reduces the fuel surface temperature.

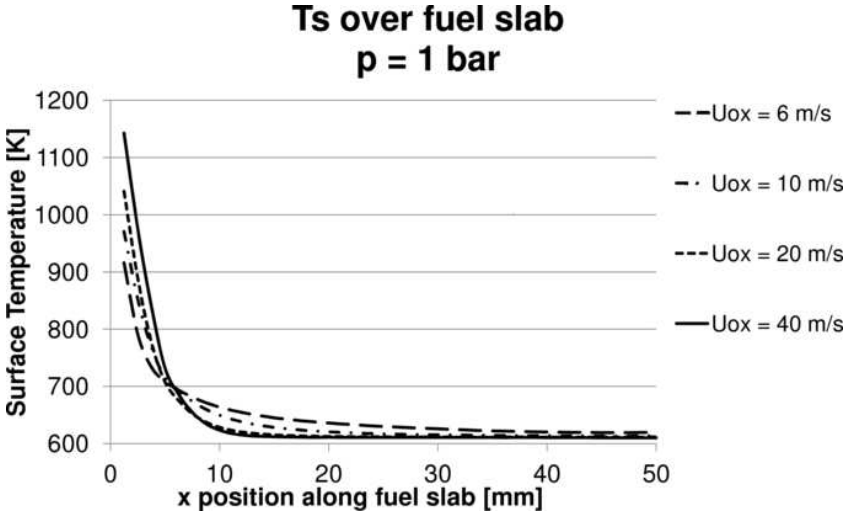

FIG. 7: Fuel surface temperature: p = 1 bar, varying G_{Ox}.

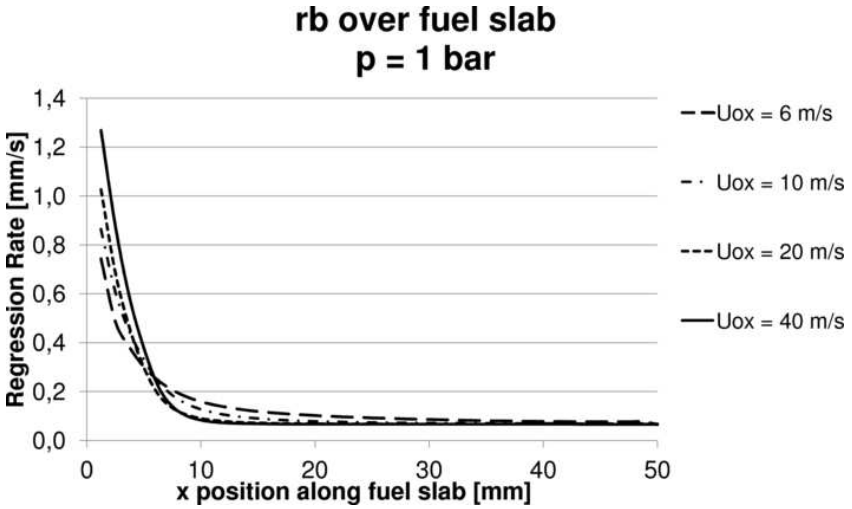

FIG. 8: Fuel regression rate: p = 1 bar, varying G_{Ox}.

Figures 9 and 10 show the fuel surface temperature and the fuel regression rate, but in this case with a fixed oxidizer mass flux G_{Ox} = 39 kg/m^2, (Re = 11,700) and a comparison of the four investigated pressures. Near the head-end side of the fuel slab, the peak temperature, and therefore the regression rate, are noticeably higher at lower pressures. On the other hand, proceeding downstream along the fuel grain an inversion of this phenomena is present: after a certain section at higher pressures corresponds higher local regression rate. This section advances toward the combustor end with de-

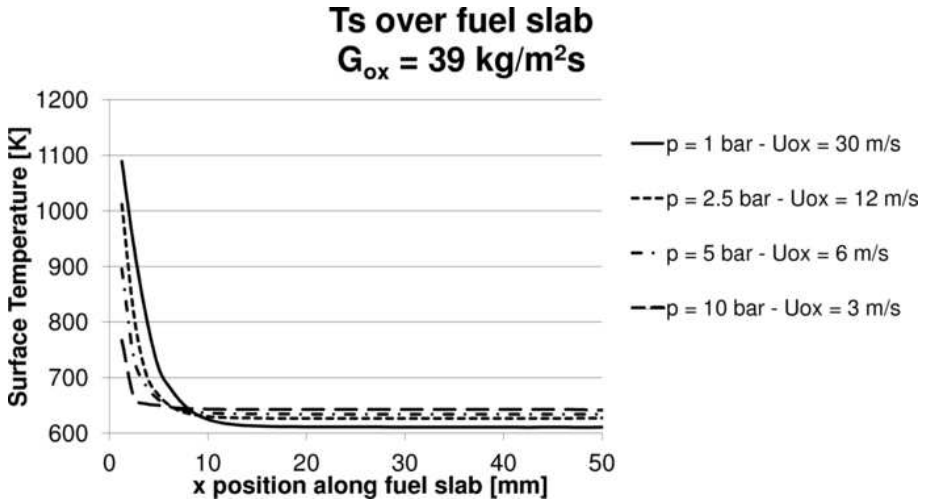

FIG. 9: Fuel surface temperature: G_{Ox} = 39 kg/m^{2}s and varying pressure.

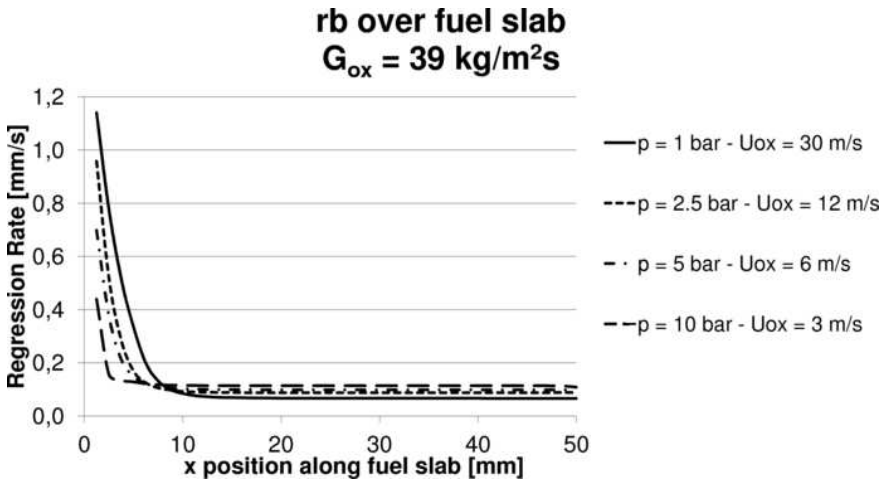

FIG. 10: Fuel regression rate: G_{Ox} = 39 kg/m^{2}s and varying pressure.

creasing pressure. This could partially explain the different experimental results present in hybrid rocket literature concerning average regression rate. In fact, the inspection of Fig. 9 and 10 shows that an increasing, decreasing, or neutral behavior can be identified with dependence on fuel grain length, pressure, and location of the regression rate measurement devices along the fuel slab. In particular, the ratio between the head-end zone length (where a local regression rate peak is noticeable) and the length of the whole fuel slab should be taken into account. It is reasonable to assume that the average regression rate of longer fuel grains will be less influenced by head-end local regression rate peaks. In addition, the position of the regression rate measurement devices could influence the average regression rate by including or excluding a different number of increasing, decreasing, or neutral local regression rate regions.

In the present work the average regression rate has been computed by numerical integration of the local regression rate over the full length of the fuel slab. Figure 11 compares the mean regression rate values at each pressure for the varying values of the oxidizer inlet mass flux. The results show that pressure has an overall reducing effect on the average regression rate and that an increase in oxidizer inlet mass flux greatly increases the average regression rate. In addition, it is noticeable that the reducing effect of pressure on the average regression rate decreases with increasing pressure. For very high pressures, a neutrally asymptotic influence of pressure increase on average regression rate is foreseeable.

Tests have been carried out to quantify the effect of modeling assumptions on the computed regression rate. In particular, for the 1 bar pressure case [condition for which the pyrolisis law of Eq. (23) is not extrapolated] regression rate results are compared for the following three cases:

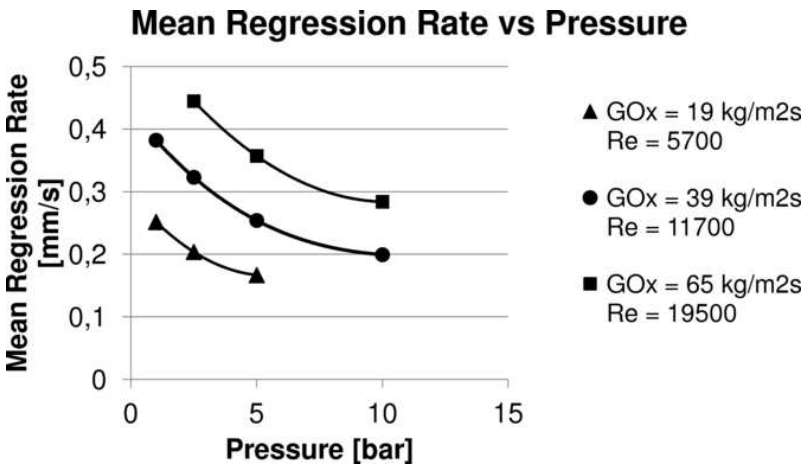

FIG. 11: Mean regression rate as a function of pressure, comparison for different oxidizer mass fluxes.

Case 1. The PSR approach is used for the computation of the chemical source term, the contribution of species enthalpy, carried by diffusion [the term $\sum_{i=1}^{Ns} \mathbf{J}_{g,i} h_{g,i}$ of Eq. (21)], to wall heat flux is neglected (Coronetti and Sirignano, 2013; Cai et al., 2013).

Case 2. The PaSR approach is used for the computation of the chemical source term and the contribution of species enthalpy, carried by diffusion, to wall heat flux is neglected.

Case 3. The PaSR approach is used and the contribution of species enthalpy, carried by diffusion, to wall heat flux is taken into account.

A comparison between case 1 and case 2 shows that the computed regression rate is, on average, 23% higher in case 2 than in case 1. The flame peak temperature region in considerably wider in the PaSR approach than in the PSR approach (Mazzetti and Barbante, 2013). This wide hot region enhances the heat flux to the wall, increasing wall temperature, and therefore the fuel regression rate. The contribution of species enthalpy, carried by diffusion, to wall heat flux has a small, albeit non negligible, effect on the fuel regression rate. The computed regression rate for case 3 is, on average, 5% higher than the regression rate computed in case 2.

Figure 12 shows a comparison between the numerical results and regression rates from literature, in which pure HTPB formulations are used as fuel grain. In order to compare a significant number of cases, different configurations (e.g., motor size, oxidizers, radial vs. slab fuel grains) are considered. Regression rate data from Sutton (Sutton and Biblarz, 2001) are for pure HTPB/GO2 (i.e., oxygen is stored in gaseous state and

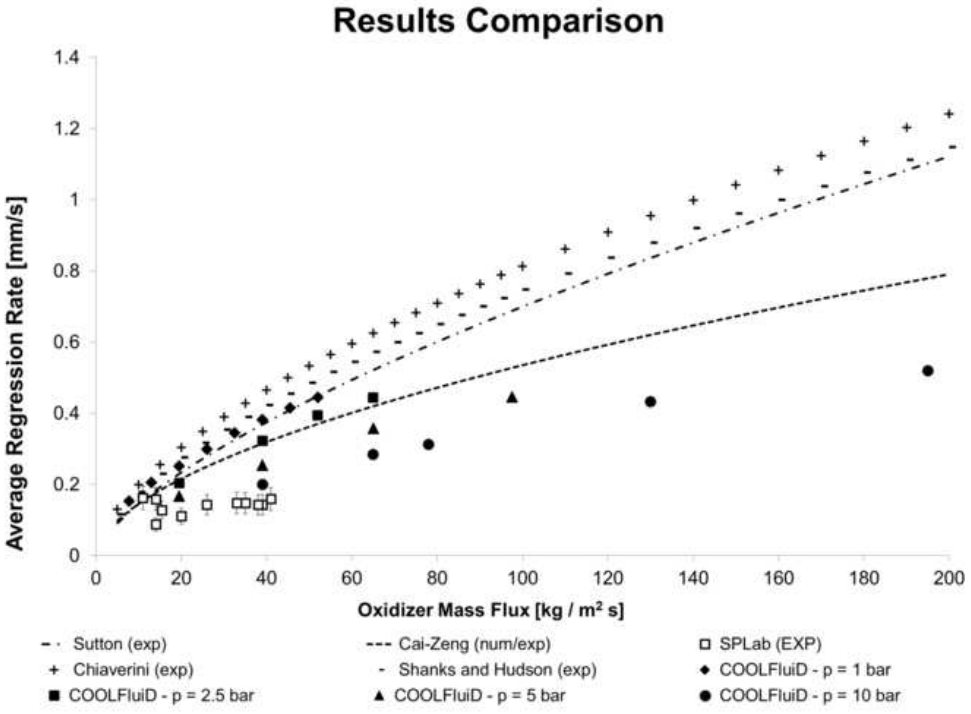

FIG. 12: Mean regression rates comparison between numerical computations and literature data. Literature data are taken from Sutton (Sutton and Biblarz, 2001), Cai-Zeng (Cai et al., 2013), SPLab (Merotto et al., 2011), Chiaverini (Chiaverini et al., 2000), Shanks and Hudson (Shanks and Hudson, 1994).

injected in such a state inside the combustion chamber) combustion in a 2 in. diameter lab-scale motor. Data from Cai-Zeng (Cai et al., 2013) are for a HTPB/H2O2 25 mm inner diameter lab-scale motor. Although in this case the oxidizer is hydrogen peroxide, the simplified reaction scheme used by the authors [the same of Venkateswaran and Merkle (1996)] does not take into account separately the combustion of excess hydrogen and it is in practice equivalent to the combustion of HTPB with gaseous oxygen. Data from SPLab (Merotto et al., 2011) are for a single slab HTPB/GO2 lab-scale combustor with a 5 mm high combustion port. Regression data from Chiaverini (Chiaverini et al., 2000) are for a double-slab HTPB/GO2 lab-scale combustor with a 9.5–12.5 mm high combustor port; Amroc (Chiaverini et al., 2000) results represent the classical correlation for a HTPB/LO2 (i.e., oxygen in stored in liquid state) large-scale 75 in. diameter hybrid rocket. Finally Shanks and Hudsons (1994) results are for a HTPB/GO2 2 in. diameter lab-scale motor. Again, it is noticeable, from our computed data, that an increase of pressure has a decreasing effect on mean regression rate and that an increase

of oxidizer inlet mass flux has an increasing effect on average fuel regression rate. As shown in Mazetti (2010), the range of oxidizer inlet mass flux investigated extends over the typical range of single-slab fuel configurations, and the maximum value shown, near 200 kg/m^{2}s, is close to the maximum value reached by experimental facilities. Even if an accurate modeling of governing equation and regression rate boundary condition are implemented, the pressure dependence of regression rate is in good accord with pyrolisis results from Risha et al. (1998), while in actual motor firings the regression rate is found to be generally independent from pressure. An inspection of Fig. 10 shows a peak of the regression rate close to the fuel head-end region for low pressure values. The regression rate peak is very sensitive to pressure changes, and its decrease with pressure accounts for the computed behavior of mean regression rate. This result is possibly related to the extrapolation of the pyrolisis law [see Eq. (23)] for pressures above 1 bar and to the assumption that in the inlet region turbulence is fully developed and the recirculation region at the combustor head end is not present.

7. CONCLUSIONS

A numerical tool for the simulation of combustion processes occurring in hybrid rocket engine combustion chambers has been developed based on the COOLFluiD code. The first innovative feature of this work is the self-consistent modeling of turbulent transport of mixture total enthalpy. This choice is made in order to overcome the possible source of inaccuracy due to the use of a single, specific heat-dependent term for the closure. The second innovative feature involves the use of a multitime partially stirred reactor model for the evaluation of turbulent chemical reaction rates in hybrid rocket engines. Thanks to this, the pseudolaminar combustion hypothesis is surpassed and it is possible to analyze fully turbulent combustion processes. An accurate boundary condition at the gas-solid fuel interface is introduced. It also accounts for the effect of chemical species enthalpy carried by diffusion at the fuel surface, an approach which is not often performed in literature works.

Computations are performed in order to estimate both local and average solid fuel regression rates. The effect of the oxidizer inlet mass flux and pressure on regression rate has been assessed. The effects of pressure on hybrid rocket combustion processes and therefore on local and average regression rate are still an open research problem. As discussed, different results are available in literature; even if conflicting, they are all scientifically sound and need to be considered carefully within their respective limits. In particular, the average regression rate measurement could be affected by several factors, such as the length of fuel grain and the sampling measurement positions. Simulated test cases for a hybrid rocket combustion chamber show a decrease in average fuel regression rate with an increase in pressure (within the 1–10 bar range). This is in agreement with pyrolisis experiments available in literature (Risha et al., 1998), while a practically pressure independent regression rate is demonstrated in many actual motors. This suggests

that further improvements of the model, like taking into account the recirculation zone at the fuel inlet, are needed. In addition, the general trend that assesses a peak in local regression rate in the fuel head-end region is confirmed.

REFERENCES

Amini, B. and Khalegi, H., A comparative study of variant of turbulence modeling in the physical behaviors of diesel spray combustion, *Therm. Sci.*, vol. **15**, no. 4, pp. 1081–1093, 2011.

Balay, S., Gropp, W. D., Curfman McInnes, L., and Smith, B. F., Efficient management of parallelism in object oriented numerical software libraries, in *Modern Software Tools in Scientific Computing*, pp. 163–202, Birkhäuser, Switzerland, 1997.

Cai, G., Zeng, P., Li, X., Tian, H., and Yu, N., Scale effect of fuel regression rate in hybrid rocket motor, *Aerosp. Sci. Technol.*, vol. **24**, pp. 141–146, 2013.

Chen, Y. S., Chou, T. H., Gu, B. R., Wu, J. S., Wu, B., Lian, Y. Y., and Yang, L., Multi-physics simulations of rocket engine combustion, *Comput. Fluids*, vol. **45**, no. 1, pp. 29–36, 2011.

Chiaverini, M. J., Harting, G. C., Lu, Y. C., Kuo, K. K., Peretz, A., Jones, S. H., Wygle, B. S., and Arves, J. P., Pyrolysis behavior of hybrid-rocket solid fuels under rapid heating conditions, *J. Propul. Power*, vol. **15**, no. 7, pp. 888–895, 1999.

Chiaverini, M. J., Serin, N., Johnson, D. K., Lu, Y. C., and Risha, G. A., Regression rate behavior of hybrid rocket solid fuels, *J. Propul. Power*, vol. **16**, no. 1, pp. 125–132, 2000.

Chiaverini, M. J., Kuo, K. K., Peretz, A., and Harting, G. C., Regression rate and heat-transfer correlations for hybrid rocket combustion, *AIAA J.*, vol. **17**, no. 1, pp. 99–110, 2007.

Coronetti, A. and Sirignano, W. A., Numerical analysis of hybrid rocket combustion, *J. Propul. Power*, vol. **29**, no. 2, pp. 371–384, 2013.

De Luca, L. T., Galfetti, L., Colombo, G., Maggi, F., Bandera, A., Boiocchi, M., Gariani, G., Merotto, L., Paravan, C., and Reina, A., Time-Resolved Burning of Solid Fuels for Hybrid Rocket Propulsion, in *EUCASS Advances in Aerospace Sciences*, Torus Press and EDP Sciences, Moscow, pp. 405–426, 2011.

Evans, B., Boyer, E., Kuo, K. K., Risha, G. A., and Chiaverini, M. J., Hybrid rocket investigations at Penn State University's high pressure combustion laboratory: Overview and recent results, in *Proc. of the 45th AIAA/ASME/SAE/ASEE Joint Propulsion Conf. and Exhibit* AIAA Paper no. 2009–3549, Denver, CO, Aug. 2-5, 2009.

Ferziger, J. H. and Kaper, H. G., *Mathematical Theory of Transport Processes in Gases*, North Holland, Amsterdam, 1972.

Gatski, T. B. and Bonnet, J. P., *Compressibility, Turbulence, and High Speed Flow*, Elsevier, Amsterdam, 2009.

Golovitchev, V. I., *Development of Universal Model of Turbulent Spray Combustion*, TFR research proposal, Chalmers University of Technology, Gothenburg, Sweden, 2001.

Golovitchev, V. I. and Chomiak, J., Numerical modeling of high temperature air flameless combustion, in *The 4th Int. Symposium on High Temperature Air Combustion and Gasification*, Rome, Italy, Nov. 26-30, 2001.

Hu, J., Xia, Z., Wang, D., and Huang, L., Numerical simulation of fuel regression rate behavior of hybrid rocket motors, *Trans. J. Soc. Aeronautic. Space Sci.*, vol. **56**, no. 6, pp. 351–359, 2013.

Jones, W. P. and Lindsted, R. P., Global reaction schemes for hydrocarbon combustion, *Combust. Flame*, vol. **73**, pp. 233–249, 1983.

Kataoka, I., Local instant formulation of two-phase flow, *Int. J. Multiphase Flow*, vol. **12**, no. 5, pp. 745–758, 1986.

Kuo, K. K. and Houim, R. W., Theoretical modeling and numerical simulation challenges of combustion processes of hybrid rockets, *The 47th AIAA/ASME/ASEE Joint Propulsion Conf. and Exhibit*, AIAA Paper 2011-5608, San Diego, CA, July 31-Aug. 3, 2011.

Lani, A., *An Object Oriented and High Performance Platform for Aerothermodynamics Simulation*, PhD Thesis, Université Libre de Bruxelles and von Karman Institute for Fluid Dynamics, Belgium, 2008.

Law, C. K., *Combustion Physics*, Cambridge University Press, Cambridge, UK, 2006.

Lewin, A., Dennis, J., Conley, B., and Suzuki, D, Experimental determination of performance parameters for a polybutadiene/oxygen hybrid rocket, *The 28th Joint Propulsion Cof. and Exhibit*, AIAA Paper 1992-3590, Nashville, TN, July 6-8, 1992.

Li, X., Tian, H., and Cai, G., Numerical analysis of fuel regression rate distribution characteristics in hybrid rocket motors with different fuel types, *Sci. China Technol. Sci.*, vol. **56**, no. 7, pp. 1807–1817, 2013.

Liou, M. S., A sequel to Ausm, Part II: AUSM+-UP, *J. Comput. Phys.*, vol. **214**, pp. 137–170, 2006.

Marxman, G. A., Wooldridge, C. E., and Muzzy, R. J., Fundamentals of hybrid boundary layer combustion, AIAA Paper 1963-505, 1963.

Mazzetti, A., *Indagine Teorica e Sperimentale dei Processi di Combustione Eterogenea in Endoreattore Ibrido*, MS Thesis, Politecnico di Milano, Aerospace Engineering Department, Milano, Italy, 2010.

Mazzetti, A. and Barbante, P. F., Object oriented techniques for the numerical simulation of combustion processes in hybrid rocket engines, in *The 5th European Conf. for*

Aeronautics and Space Sciences, Munich, Germany, July 1-5, 2013.

Menter, F. R., Two-equation eddy-viscosity turbulence models for engineering applications, *AIAA J.*, vol. **32**, no. 8, pp. 1598–1605, 1994.

Merotto, L., Boiocchi, M., Mazzetti, A., Maggi, F., Galfetti, L., and De Luca, L. T., Characterization of a family of paraffin-based solid fuels, in *The 4th European Conf. for Aeronautics and Space Sciences*, St. Petersburg, Russia, July 4-8, 2011.

Nordin, N., *Complex Chemistry Modeling of Diesel Spray Combustion*, PhD Thesis, Chalmers University of Technology, Gothenburg, Sweden, 2001.

Price, C. F. and Smoot, L. D., Regression rates of nonmetalized hybrid fuel systems, *AIAA J.*, vol. **3**, pp. 1408–1413, 1965.

Quintino, T., *A Component Environment for High-Performance Scientific Computing – Design and Implementation*, PhD Thesis, Katolieke Universiteit Leuven and von Karman Institute for Fluid Dynamics, Belgium, 2008.

Ramshaw, J. D., Self-consistent effective binary diffusion in multicomponent gas mixtures, *J. Non-Equilib. Thermodyn.*, vol. **15**, pp. 295–300, 1990.

Risha, G. A., Harting, G. C., Kuo, K. K, Peretz, A., Kochand, D. E., Jones, H. S., and Arves, J. P., Pyrolysis and combustion of solid fuels in various oxidizing environments, *The 34th AIAA/ASME/AEA/ASEE Joint Propulsion Conf.*, AIAA Paper 1998-3184, Cleveland, OH, July 13-15, 1998.

Sabelnikov, V. and Fureby, C., LES combustion modeling for high Re flames using a multi-phase analogy, *Combust. Flame*, vol. **160**, pp. 83–96, 2013.

Shanks, R. B. and Hudson, M. K., The design and control of a labscale hybrid rocket facility for spectroscopy studies, *The 30th Joint Propulsion Conf.*, AIAA Paper 1994-3016, Colorado Springs, CO, June 20-23, 1994.

Sun, X., Tian, H., Yu, N., and Cai, G., Regression rate and combustion performance investigation of aluminum metallized htpb/98hp hybrid rocket motor with numerical simulation, *Aerospace Sci. Technol.*, vol. **42**, pp. 287–296, 2012.

Sutton, G. P. and Biblarz., O., *Rocket Propulsion Elements*, 7th ed., Wiley, New York, 2001.

Venkateswaran, S. and Merkle, C. L., Size scale-up in hybrid rocket motors, *The 34th Annual Aerospace Sciences Meeting and Exhibit*, AIAA Paper 1996-647, Reno, NV, July 15-18, 1996.

Veynante, D. and Poinsot, T., *Theoretical and Numerical Combustion*, Cerfacs, Toulouse, France, 2011.

Veynante, D. and Vervisch, L., Turbulent combustion modeling, *Prog. Energy Combust. Sci.*, vol. **28**, pp. 193–266, 2002.

Wilcox, D. C., *Turbulence Modeling for CFD*, DCW Industries Inc., La Canada, CA, 2006.

Wuilbaud, T., *Algorithmics Developments for a Multiphysics Framework*, PhD Thesis, Université Libre de Bruxelles and von Karman Institute for Fluid Dynamics, Belgium, 2008.

Yash, P., Kalpit, K., and Dash, P. K., Regression rate study of PVC/HTPB hybrid rocket fuels, *Int. J. Mech. Indust. Eng.*, vol. **1**, no. 1, pp. 64–67, 2011.